Rotationally resolved single-photon ionization of HCl and DCl

M. Drescher, A. Brockhinke, N. Böwering, and U. Heinzmann
Universität Bielefeld, Fakultät für Physik, D-4800 Bielefeld 1, Germany

H. Lefebvre-Brion
Laboratoire de Photophysique Moléculaire, Bâtiment 213, Université de Paris-Sud, 91405 Orsay Cedex, France

(Received 14 April 1993; accepted 30 April 1993)

The rotationally resolved photoionization yields of jet-cooled HCl and DCl have been measured in the energy range between their spin–orbit split $^2\Pi$ ionic thresholds. For single-photon excitation, narrow-band vuv radiation is generated by resonant frequency mixing. The spectra are complex due to an interaction of autoionizing resonances belonging to series converging to different rotational states of the ion core. This is taken into account using the multichannel quantum defect theory in a treatment capable to handle a transition in angular momentum coupling from Hund's case (c) to case (e). Even for Rydberg orders $n>35$ the experimental data cannot be explained using a pure case (e) picture.

I. INTRODUCTION

In studies of molecular ionization based on monochromatized light from synchrotron radiation or discharge lamp sources the limitation of resolving powers to values $<10^4$ did not allow the spectral resolution of rotational structure.[1] Especially the near-threshold regions are often influenced by complex interactions between the motion of the excited Rydberg electrons and the vibration and rotation of the ionic cores, leading to a rich structure of autoionization resonances in photoelectron yield spectra. This is also the case for the photoionization cross section of HCl, which has previously been measured at a wavelength resolution of 0.007 nm employing a helium continuum light source.[2]

The development of laser-based frequency mixing techniques[3] now provides the experimentalist with resolving powers $>10^5$ and high photon fluxes ($>10^{10}$/s). This is ideally suited for the study of the photoionization dynamics of molecules.[4–7] The improvements in experimental resolution have been accompanied by further development of a theoretical treatment taking into account the variation of the angular momentum coupling when the principal quantum number n of the Rydberg electron increases.[8]

A previous investigation of the spin–orbit autoionization of HI has exhibited a transition from Hund's coupling case (c) to case (e) for sufficiently high Rydberg orders ($10<n<15$) in the experimental data as well as in the calculation.[9] In this paper we report a similar investigation for the spin–orbit autoionization region of the halides HCl and DCl. Here the energy splitting between the lowest order Rydberg levels ($n>13$) is already of the same magnitude as the spacing between successive rotational states of the ion, making these molecules suitable targets for the study of Hund's case (e) coupling.[8,10,11]

II. EXPERIMENT

In contrast to HI,[9] where the ionizing radiation with wavelengths of $\lambda>111$ nm lies well above the transmission cutoff of LiF windows, the ionization of HCl and DCl with $\lambda<97.4$ nm requires a windowless frequency mixing technique: Two laser beams of frequencies ω_r and ω_t are focused collinearly into a pulsed jet of xenon to generate light of the sum frequency $\omega_{vuv}=2\omega_r+\omega_t$ (Ref. 12) (Fig. 1). The laser beam of frequency ω_r is produced by frequency doubling of the output of a Nd:YAG pumped dye laser (Quanta Ray PDL 2, operated with Coumarin 120 at 10 Hz) in a BBO crystal. Tuning this wavelength to the $6p'(1/2,0)$ two-photon resonance in Xe at 222.6 nm results in a strong enhancement of the intensity at the sum frequency.

A second dye laser (Lambda Physik FL 3002, operated with Styril 8) is tuned to wavelengths λ_t between 730 and 780 nm, giving rise to vuv radiation in the range of 96.6 to 97.4 nm. The separation of the sum-frequency light from the fundamentals and the difference-frequency $2\omega_r-\omega_t$ is performed by a differentially pumped monochromator, consisting of a spherical mirror and a spherical grating, blazed for 90 nm, in a Wadsworth configuration. Both optical elements are coated with platinum and used near normal incidence; thus the beam direction as well as the state of polarization are almost conserved. The transmission at the sum frequency is calculated to be >2%. With input energies of 0.5 mJ at ω_r and 5 mJ at ω_t a vuv photon flux up to 10^9/pulse has been measured behind the monochromator. The refocused vuv light intersects a pulsed supersonic beam of target molecules seeded in neon and differentially pumped using a skimmer.

Different mixtures of HCl with the rare gases helium, neon, and argon have been tested. The best cooling effect has been found for 5% HCl in neon. Lower concentrations of target molecules gave no further improvement. During operation of the jet a 300 ℓ/s turbomolecular pump maintains a pressure of 1.5×10^{-6} mbar in the ionization region. Photoionization takes place in an extraction field inside a stainless steel cage consisting of a cylinder (56 mm inner diam.) and two end caps formed by hemispheres of same diameter with a distance of 100 mm between their centers. The cylinder and the two spheres are maintained at potentials of −30, 0, and −6 V, respectively, resulting in a field

 0021-9606/93/99(4)/2300/7/$6.00

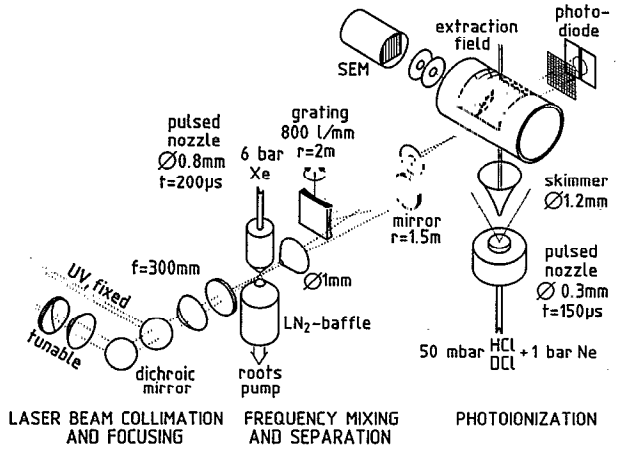

FIG. 1. Experimental setup for the measurement of the photoionization yield of molecules after excitation with vuv light, generated by resonant sum-frequency mixing in xenon.

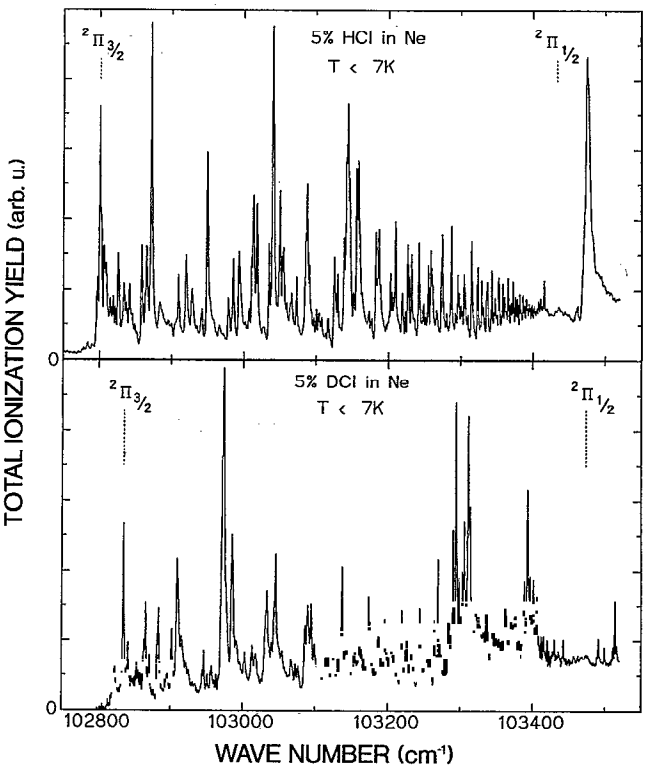

FIG. 2. Total ionization yields of rotationally cooled HCl (upper spectrum) and DCl (lower spectrum) in the autoionization region between the $^2\Pi$ spin–orbit components of the ions.

strength of approx. 0.5 V/cm at the position of ionization.

All produced electrons in the ionization region are directed through a hole in the sphere held at ground potential onto an electron multiplier tube while background electrons emitted from the cage walls are suppressed. Behind the target a horizontally split dual vacuum photodiode serves for optical alignment and normalization of the photoelectron signal to the vuv intensity. This is important because the scanning range coincides with an autoionization resonance of Xe causing a strong variation of the vuv yield when the wavelength is scanned. Spectra were created by linking together subsequent scans of 120 cm^{-1} length. Each data point is the mean value of 50 to 100 laser shots. The wave number was incremented in steps of 0.3 cm^{-1}. For constant expansion conditions of the molecular beam the spectra were reproducible within the limits of the experimental uncertainty.

III. EXPERIMENTAL RESULTS

In Fig. 2 we present the relative total photoionization cross sections of HCl and DCl in a range of photon energies dominated by autoionization of Rydberg levels which converge to the $^2\Pi_{1/2}$ ionic state and decay into the continuum of the $^2\Pi_{3/2}$ ion states. The statistical error for each data point is typically 1% for HCl and 2% for DCl.

From the narrowest features in the spectra an upper limit for the vuv bandwidth of 1 cm^{-1} can be estimated. In a previous experiment on HCl (Ref. 13) utilizing nonresonant frequency tripling in Xe the absolute wave number positions of the observed peaks have been determined to an accuracy of ± 1 cm^{-1} by monitoring the fluorescence of I_2 excited by the fundamental laser beam. Although this spectrum exhibited larger statistical errors it served to establish the wave number scale of the present HCl spectrum.

By using a mixture of HCl and DCl this scale could also be extended to the DCl spectrum. Due to the skimmed supersonic expansion of the molecules transitions starting from rotational levels of the ground state with $J''>0$ are strongly suppressed. Assuming a Boltzmann distribution a rotational temperature of less than 7 K can be determined. This temperature is much lower than the value of 130 K, given for the spectrum of HCl reported in Ref. 2. Therefore, that spectrum is quite different from the present one, since there levels of the ground state up to $J''=5$ were populated significantly. Although in our experimental results only $R(0)$ lines contribute appreciably, the spectra are nevertheless very dense even in the vicinity of the lower thresholds. This high line density is caused by several series with different electronic angular momentum l converging to ionic states with different total angular momentum J^+ as illustrated in Fig. 3.

The peak heights exhibit irregular fluctuations with increasing energy rather than a steady decrease as it is normally found in Rydberg progressions. The line profiles of the autoionization resonances are found to be asymmetric for low Rydberg orders, where the natural linewidth is larger than the bandwidth of the vuv radiation. The spectra of HCl and DCl cover almost the same range of wave numbers. Nevertheless, they are of strikingly different appearance. The sharp onsets at the $^2\Pi_{3/2}$ thresholds are shifted from their true positions to smaller wave numbers due to field-induced ionization in the extraction field with a field strength of approx. 0.5 V/cm. By lowering the field strength to 0.025 V/cm the ionization thresholds were found to be 102 801.5 ± 1 cm^{-1} for HCl and 102 836.1 ± 1 cm^{-1} for DCl. These results agree well with values found in zero kinetic energy (ZEKE) experiments yielding

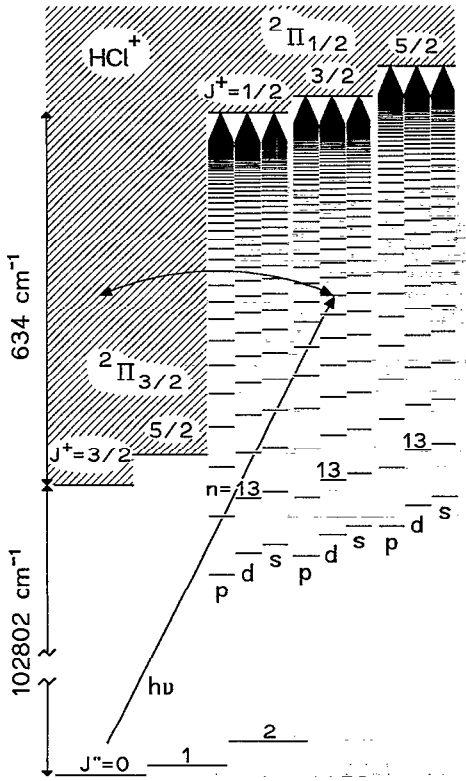

FIG. 3. Scheme of autoionization in HCl and DCl for a case (e) situation: Series with different electron angular momentum l converge to thresholds with different total angular momentum J^+ of the ion.

102 798.3 cm^{-1},[14] or 102 802.8±2 cm^{-1},[15] (HCl), and 102 836.1 cm^{-1},[14] (DCl). Those investigations also provided data for the $^2\Pi_{1/2}$ ionization limits, whereas in our spectra no distinct features can directly be attributed to these thresholds.

IV. CALCULATIONS

The spectra of the total photoionization yields of HCl and DCl were calculated using the multichannel quantum defect theory (MQDT) by describing the final states in an angular momentum coupling case intermediate between Hund's cases (c) and (e). The program used previously for calculations on HI (Ref. 9) was modified to introduce mixing between s and d states. This mixing is obtained from *ab initio* calculations,[2] but in order to simplify, the mixing coefficients were taken the same for singlet and triplet states and were renormalized in the following way:

$$s\sigma = 0.9340 s\sigma + 0.3572 d\sigma,$$

$$d\sigma = -0.3572 s\sigma + 0.9340 d\sigma.$$

Other l mixings, such as $p\pi$–$d\pi$ mixing, were neglected.

The values for the quantum defects are crucial for the assignments of the peaks. They were slightly modified from previously calculated-*ab initio* values[2] in order to achieve good agreement with the spectra obtained in a two-color laser experiment[16] with a $D\,^1\Pi$ $4p\sigma$ intermediate state. These modified values were taken here since the final states are practically the same in the two experiments. However, for a single-photon transition from the $X\,^1\Sigma^+$ ground state mainly final states with values $J'=1$ can be reached, because only $R(0)$ lines are intense due to the low rotational temperature of 7 K. On the other hand, starting from the selected $D\,^1\Pi$ state with $J''=1$, two levels $J'=1,2$ can be populated. The transition moments from $X\,^1\Sigma^+$ are based on *ab initio* calculations,[2] but for better agreement with the observed intensities, the transition moment to the $s\sigma$ states was divided by two. A comparison between calculated and observed peak positions is given for Rydberg orders $13 \leqslant n \leqslant 18$ for HCl in Table I and for DCl in Table II.

V. DISCUSSION

For a closer examination we will focus on two spectral regions.

A. 13<n<18

In the range from 102 800 to 103 100 cm^{-1} successive Rydberg levels are well separated, thus allowing a comparison between observed and calculated line positions. In Table I (HCl) and Table II (DCl) we list the calculated resonance energies of s, p, and d series, converging to thresholds with different total ionic angular momentum J^+. For $\Omega^+=1/2$ the case (e) rules $|J'-j| \leqslant J^+ \leqslant J'+j$ and $J^+ \geqslant \Omega^+$ (where $\mathbf{J}'=\mathbf{J}^+ + \mathbf{j}$ and $\mathbf{j}=\mathbf{l}+\mathbf{s}$) limit J^+ to the values $J^+_{min}=1/2$ and $J^+_{max}=3/2$, 5/2, and 7/2 for $l=0,1,2$, respectively, because $J'=1$ (see above).

While most observed peaks can be attributed to calculated positions (see Figs. 4 and 5), some features, especially near the $^2\Pi_{3/2}$ thresholds remain unassigned. They may arise from rotational autoionization of series converging to $^2\Pi_{3/2}$ states with $J^+ > 3/2$. The strongest contributions to the spectra arise from s and d series converging to the $\Omega^+=1/2$, $J^+=1/2$ and 3/2 limits, whereas higher J^+ values as well as the p series are of minor importance.

Due to the pronounced difference of the rotational constants of HCl ($B^+=9.79$ cm^{-1}) and DCl ($B^+=5.06$ cm^{-1}) (Ref. 17) the spectra exhibit only little similarity, although it can be seen from Table I that the mean values of quantum defects are essentially the same. With the exception of a few peaks, the difference between calculated and observed peak positions is usually less than 3 cm^{-1} for both HCl and DCl. A quantitative reproduction of the observed relative intensities and linewidths, on the other hand, seems to be more complicated. The $l=2$, $J^+=3/2$, $n=14,15$ resonances are sufficiently isolated from neighboring peaks to allow an analysis of their line shapes in terms of Fano profiles, yielding a q parameter of approximately 5 for the d series.

B. n>28 in HCl

Next, we discuss the spectral region just below the HCl^+ $^2\Pi_{1/2}$ thresholds. Referring to Fig. 6 for $\omega > 103\,350$ cm^{-1} a strikingly regular pattern becomes apparent in the HCl spectrum if one combines suitable choices of peaks together to form overlapping fringes labeled $F1$–$F4$. In DCl such enveloping structures are covered by stronger

TABLE I. Observed and calculated peak positions and related quantum defects of autoionization resonances of HCl for several Rydberg orders n of s, p, and d series converging to thresholds with different J^+ values. The ionization limits are taken from Ref. 14.

(a) $R(0)$ lines of s series for HCl from $X\,^1\Sigma^+$ ground state.

n	obs. w.n. (cm^{-1})	obs. μ	calc. w.n. (cm^{-1})	calc. μ	obs.-calc. w.n. (cm^{-1})
$J^+=1/2$		Limit=103 432.3 cm^{-1}			
14	102 858.8	0.167	102 858.6	0.170	0.2
15	102 935.1	0.144	102 935.2	0.142	−0.1
16	102 993.8	0.181	102 993.2	0.191	0.6
17	103 045.5	0.157	103 045.6	0.154	−0.1
$J^+=3/2$		Limit=103 461.2 cm^{-1}			
13	102 801.2	0.106	102 793.6	0.180	7.6
14	102 884.2	0.209	102 885.2	0.197	−1.0
15	102 958.4	0.227	102 960.6	0.194	−2.2
16	103 026.5	0.112	103 022.2	0.190	4.3

(b) $R(0)$ lines of p series for HCl from $X\,^1\Sigma^+$ ground state

n	obs. w.n. (cm^{-1})	obs. μ	calc. w.n. (cm^{-1})	calc. μ	obs.-calc. w.n. (cm^{-1})
$J^+=1/2$		Limit=103 431.8 cm^{-1}			
14	102 819.4	0.614	102 818.8	0.62	0.56
15	102 900.2	0.632	102 901.4	0.616	−1.2
16	102 966.5	0.643	102 967.8	0.621	−1.8
17	103 018.4	0.707	103 023.0	0.616	−4.6
$J^+=3/2$		Limit=103 462.2 cm^{-1}			
14	102 849.2	0.620	102 849.2	0.620	0.0
15	102 928.7	0.658	102 929.8	0.643	−1.1
16	102 993.9	0.692	102 996.8	0.644	−2.9
17	103 050.0	0.680	103 052.0	0.644	−1.8
$J^+=5/2$		Limit=103 510.1 cm^{-1}			
13	...	...	102 792.0	0.638	
14	102 895.5	0.638	102 895.0	0.643	0.5
15	102 978.8	0.628	102 978.0	0.639	0.8
16	...	...	103 044.6	0.646	

(c) $R(0)$ lines of d series for HCl from $X\,^1\Sigma^+$ ground state

n	obs. w.n. (cm^{-1})	obs. μ	calc. w.n. (cm^{-1})	calc. μ	obs.-calc. w.n. (cm^{-1})
$J^+=1/2$		Limit=103 432.3 cm^{-1}			
14	102 845.2	0.328	102 850.2	0.270	−5.0
15	102 928.8	0.237	102 930.4	0.213	−1.6
16	102 985.7	0.325	102 988.6	0.274	−2.9
17	103 040.9	0.265	103 040.6	0.262	0.3
$J^+=3/2$		Limit=103 461.2 cm^{-1}			
14	102 872.1	0.352	102 875.0	0.318	−2.9
15	102 949.7	0.353	102 952.0	0.320	−2.3
16	103 013.5	0.344	103 015.0	0.318	−1.5
17	103 066.0	0.336	103 066.8	0.320	−0.8
$J^+=5/2$		Limit=103 512.4 cm^{-1}			
13	102 834.3	0.279	102 831.8	0.302	2.5
14	102 928.5	0.291	102 925.4	0.327	3.1
15	103 002.2	0.334	103 003.6	0.314	−1.4
16	103 059.2	0.439	...	...	
$J^+=7/2$		Limit=103 579.7 cm^{-1}			
13	102 895.6	0.335	102 900.4	0.290	−4.8
14	102 993.8	0.314	102 995.2	0.298	−1.4

features due to perturbations, probably induced by low Rydberg states converging to higher electronic or vibrational thresholds.

The phenomenon of fringe formation has previously been described for high Rydberg states of Na_2 (Ref. 18) and NO (Ref. 19) and has been attributed to a "stroboscopic" effect between the movement of the Rydberg electron and the ion rotation or to a particular situation for the transition moments and phases of an l-mixing, respectively.

The treatment of each fringe as a separate Rydberg series leads to fitted quantum defects and ionization limits as given in Table III. However, these limits are not consistent with the values from Refs. 14 and 15 even if one assumes a simultaneous shift of a few cm^{-1}. In particular, no series converging to the $J^+=1/2$ limit (approximately 103 433 cm^{-1}) can be found. In order to investigate the

TABLE II. Observed and calculated peak positions and related quantum defects of autoionization resonances of DCl for several Rydberg orders n of s, p and d series converging to thresholds with different J^+ values. The ionization limits are taken from Ref. 14.

n	obs. w.n. (cm^{-1})	obs. μ	calc. w.n. (cm^{-1})	calc. μ	obs.-calc. w.n. (cm^{-1})
(a) $R(0)$ lines of s series for DCl from $X\,^1\Sigma^+$ ground state					
$J^+=1/2$		Limit=103 474.6 cm^{-1}			
14	102 902.5	0.150	102 899.6	0.185	2.9
15	102 973.5	0.202	102 974.8	0.182	−1.3
16	103 034.0	0.218	103 036.4	0.175	−2.4
17	103 086.6	0.183	103 087.0	0.174	−0.4
$J^+=3/2$		Limit=103 488.9 cm^{-1}			
14	102 915.7	0.164	102 913.8	0.186	1.9
15	102 992.0	0.139	102 989.0	0.184	3.0
16	103 050.1	0.186	103 050.6	0.177	−0.5
17	103 099.7	0.209	103 100.0	0.202	−0.3
(b) $R(0)$ lines of p series for DCl from $X\,^1\Sigma^+$ ground state					
n	obs. w.n. (cm^{-1})	obs. μ	calc. w.n. (cm^{-1})	calc. μ	obs.-calc. w.n. (cm^{-1})
$J^+=1/2$		Limit=103 473.9 cm^{-1}			
14	102 860.7	0.623	102 860.6	0.624	0.1
15	102 944.8	0.599	102 943.0	0.623	1.8
16	103 013.5	0.561	103 009.8	0.623	3.7
17	103 067.2	0.574	103 064.8	0.622	2.2
18	103 112.1	0.584	103 110.6	0.620	1.5
$J^+=3/2$		Limit=103 490.2 cm^{-1}			
14	102 874.1	0.654	102 874.8	0.646	−0.7
15	102 957.5	0.657	102 957.6	0.646	−0.1
16	103 026.5	0.616	103 024.8	0.645	1.7
17	103 077.0	0.704	103 080.0	0.645	−3.0
$J^+=5/2$		Limit=103 514.1 cm^{-1}			
14	102 902.5	0.605	102 899.6	0.637	2.9
15	102 980.0	0.666	102 980.6	0.658	−0.6
16	103 050.0	0.623	103 050.6	0.613	−0.6
17	103 104.7	0.628	103 105.8	0.606	−1.8
(c) $R(0)$ lines of d series for DCl from $X\,^1\Sigma^+$ ground state					
n	obs. w.n. (cm^{-1})	obs. μ	calc. w.n. (cm^{-1})	calc. μ	obs.-calc. w.n. (cm^{-1})
$J^+=1/2$		Limit=103 474.6 cm^{-1}			
14	102 892.6	0.269	102 890.6	0.292	2.0
15	102 967.6	0.288	102 969.0	0.268	−1.4
16	103 031.7	0.259	103 030.0	0.289	1.7
17	103 085.5	0.206	103 082.2	0.277	3.3
$J^+=3/2$		Limit=103 488.9 cm^{-1}			
14	102 902.5	0.320	102 903.8	0.305	−1.3
15	102 978.2	0.341	102 980.6	0.307	−2.4
16	103 045.9	0.261	...	...	
17	103 095.1	0.307	103 095.0	0.309	0.1
$J^+=5/2$		Limit=103 516.0 cm^{-1}			
13	102 835.9	0.298	102 838.4	0.274	−2.5
14	102 931.4	0.299	102 933.2	0.278	−1.8
15	103 012.2	0.241	103 009.0	0.288	3.2
16	103 069.1	0.330	103 071.2	0.293	−2.1
$J^+=7/2$		Limit=103 549.5 cm^{-1}			
13	102 871.7	0.276	102 872.0	0.273	−0.9
14	102 963.9	0.311	...	...	
15	103 040.6	0.316	103 043.4	0.275	−2.8

influence of the bandwidth of the vuv radiation which dominates the linewidths of the observed peaks in this region, we simulated the spectrum [Fig. 7(c)] using a simple model: The resonance positions for the s and d series converging to thresholds with $J^+=1/2$ and 3/2 were calculated using the Rydberg formula, $E=Ip(J^+)-R/\nu^2$, where R is the mass-corrected Rydberg constant for HCl. The quantum defects were taken as the mean values from the MQDT calculation, $\mu=0.17$ ($l=0$) and $\mu=0.31$ ($l=2$). The separations between successive rotational ionization limits $Ip(J^+)$ and $Ip(J^++1)$ were taken from Ref. 14. The line shape was approximated by a Gaussian profile

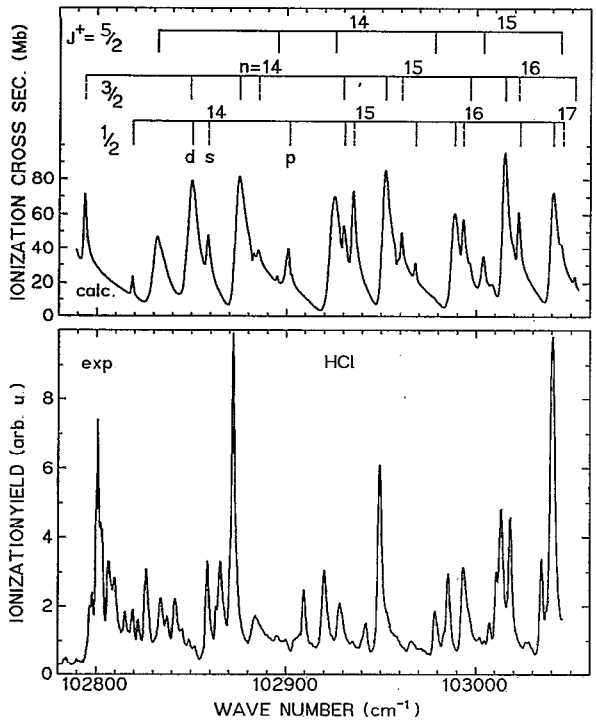

FIG. 4. Comparison of the experimental data for HCl (lower spectrum) with the result of the MQDT calculation (upper frame). The assignments of the experimental peaks are given in Table I.

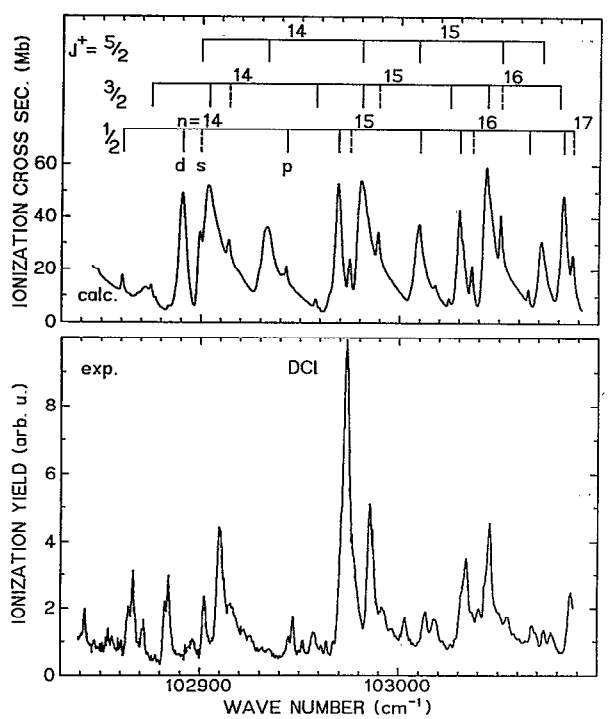

FIG. 5. Comparison of the experimental data for DCl (lower spectrum) with the result of the MQDT calculation (upper frame). The assignments of the experimental peaks are given in Table II.

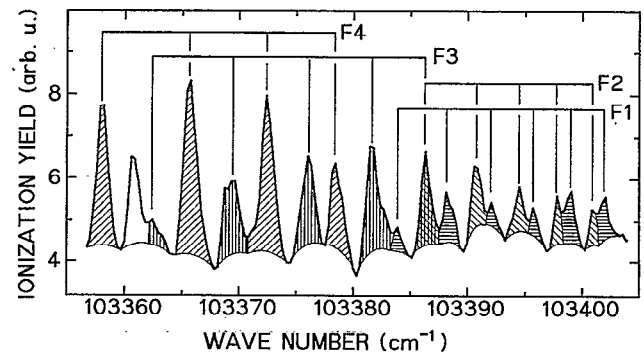

FIG. 6. Ionization yield of HCl in the region below the $J^+=1/2$ ionization threshold. Overlapping regular patterns become obvious when peaks are combined to form fringes $F1$–$F4$.

with a constant width of 1 cm^{-1} while the intensities were scaled according to a $1/n^3$ law.

As seen from a comparison of Figs. 7(b) and 7(c), for wave numbers $>103\,365$ cm^{-1} this simulation reproduces the overall structure of the observed spectrum quite well. Best agreement with the experimental data is obtained with an ionization limit $I_p(1/2)$ of $103\,438.8\pm2$ cm^{-1} which differs considerably from the values of $103\,432\pm1$ cm^{-1} given in Ref. 20 and $103\,434.7\pm2$ cm^{-1} from Ref. 15. For smaller wave numbers only a few peaks are simulated correctly indicating that a description in terms of an unperturbed Rydberg progression fails even for Rydberg orders $n>28$.

In a more elaborated approach the MQDT formalism (see Sec. IV) was used to calculate this part of the spectrum. The high spectral density is reduced after convolution with a bandwidth of 1 cm^{-1} [Fig. 7(a)]. To improve the agreement between experimental and calculated spectra the spectrum had to be shifted again by 6.5 cm^{-1}. This could be due to the inprecision of the calculation. In contrast to Refs. 18 and 19 here the appearance of fringes is an effect of the finite resolution, which becomes comparable to the separation between adjacent peaks with $J^+=1/2$ and 3/2 for sufficiently high values of n [see Figs. 7(d) and 7(e), respectively].

VI. COMPARISON WITH REMPI SPECTRA

If the spectra from the (2+1) REMPI experiment of Grant and co-workers[16] are compared to the present result, their spectra appear very different from ours except for the d lines with $J^+=1/2$ and 3/2 thresholds, which are the most intense in both experimental data sets. Even the po-

TABLE III. Ionization limits and quantum defects obtained by treating the observed fringes $F1$–$F4$ (Fig. 6) in terms of Rydberg series.

Fringe	Quantum defect	Ionization limit (cm^{-1})
$F1$	0.11	103 464.5
$F2$	0.08	103 477
$F3$	0.1	103 463.5
$F4$	0.69	103 477.5

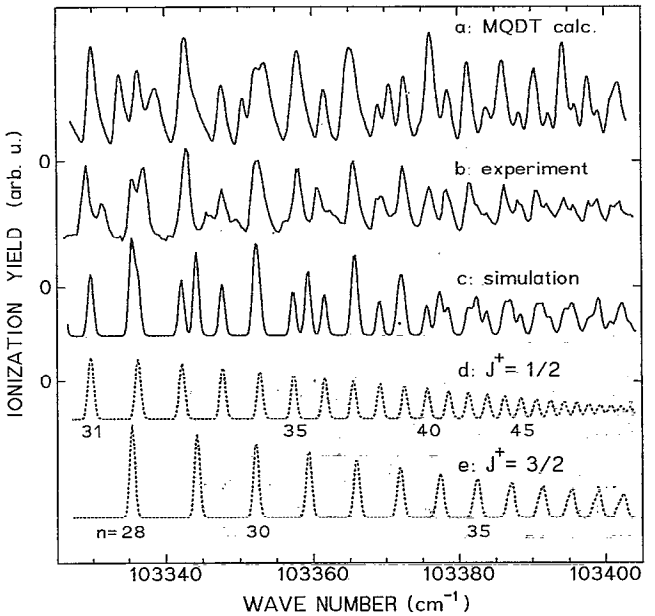

FIG. 7. Experimental spectrum of HCl (b) for high Rydberg orders, $n>28$, compared with (a) the result of the MQDT calculation and (c) a simulation based on a pure case (e) model (see text). For both (a) and (c) an ionization limit of 103 438.8 cm^{-1} was used. The contributions to the simulation from progressions converging to ionic thresholds with angular momenta of $J^+=1/2$ and 3/2 are shown separately in (d) and (e), respectively.

sitions of these peaks differ in some cases by about 2 cm^{-1}; this corresponds exactly to the calculated difference between the positions for $J'=1$ and $J'=2$ at the values of n considered here. This is reasonable since, as mentioned in Sec. IV, for the single-photon experiment the observed resonance corresponds to $J'=1$ whereas for multiphoton excitation it is often a $J'=2$ level. Some of the unassigned peaks in the vicinity of the $^2\Pi_{3/2}$ ionization limit can also be detected in the REMPI spectra and correspond probably to levels converging to high J^+ thresholds of $^2\Pi_{3/2}$. A few peaks are not seen at all in the REMPI data, for example the ones at 102 815.4 and 102 909.7 cm^{-1}. They could belong to states converging to thresholds with a vibrationally excited ion core $v^+=1$ of the $^2\Pi_{1/2}$ substate. Due to different Franck–Condon overlaps, such peaks are expected to appear slightly stronger when excited from the ground state rather than from a Rydberg state with $v=0$.

VII. CONCLUSION

The resolution of rotation in the photoionization yield spectra of HCl and DCl obtained with excitation by laser-generated vuv light enables the study of the angular momentum coupling in the autoionization of these diatomic molecules. The interaction of series converging to different ionic rotational states leads to irregular changes of the positions and amplitudes of lines. The finite resolution of the ionizing radiation simplifies the appearance of the HCl spectrum for high Rydberg orders and gives rise to the formation of fringes. A study with even higher resolution in this energy region would be useful for an assignment of the peaks without ambiguity. In any case, the correct prediction of observed structures requires an advanced theoretical treatment taking into account a transition between Hund's coupling case (c) and case (e). In general, the assignments made in this work are supported by data from a (2+1) REMPI experiment with a $D\,^1\Pi$ intermediate state.[16] Nevertheless, improvements in the prediction of the line intensities and linewidths, in particular of the d states, have to be made. A further confirmation of the assignment could be obtained from the measurement of the integral spin polarization. For the case of HI, it was demonstrated that this method yields additional information about the photoionization dynamics.[21]

ACKNOWLEDGMENTS

This work was supported by the SFB 216 of the Deutsche Forschungsgemeinschaft and by the European Community.

[1] M. L. Ginter, D. S. Ginter, and C. M. Brown, Appl. Opt. **19**, 4015 (1980).
[2] H. Lefebvre-Brion, P. M. Dehmer, and W. A. Chupka, J. Chem. Phys. **88**, 811 (1988).
[3] C. R. Vidal, Appl. Opt. **19**, 3897 (1980).
[4] A. Mank, M. Drescher, T. Huth-Fehre, G. Schönhense, N. Böwering, and U. Heinzmann, J. Electron Spectrosc. Relat. Phenom. **52**, 661 (1990).
[5] D. J. Hart and J. W. Hepburn, Chem. Phys. **129**, 51 (1989).
[6] R. G. Tonkyn, J. W. Winniczek, and M. G. White, Chem. Phys. Lett. **164**, 137 (1989).
[7] F. Merkt and T. P. Softley, Phys. Rev. A **46**, 302 (1992).
[8] H. Lefebvre-Brion, J. Chem. Phys. **93**, 5898 (1990).
[9] A. Mank, M. Drescher, T. Huth-Fehre, N. Böwering, U. Heinzmann, and H. Lefebvre-Brion, J. Chem. Phys. **95**, 1676 (1991).
[10] H. Frohlich, P. M. Guyon, and M. Glass-Maujean, J. Chem. Phys. **94**, 1102 (1991).
[11] M. Büchner, G. Raseev, and N. A. Cherepkov, J. Chem. Phys. **96**, 2691 (1992).
[12] G. Hilber, A. Lago, and R. Wallenstein, J. Opt. Soc. Am. B **4**, 1753 (1987).
[13] M. Drescher, A. Brockhinke, N. Böwering, A. Elizarov, and U. Heinzmann, in Fourth European Conference on Atomic and Molecular Physics, Riga 1992, Book of Abstracts, Vol. 16B, p. 181; and unpublished results
[14] F. R. Grant (private communication).
[15] R. G. Tonkyn, R. T. Wiedmann, and M. G. White, J. Chem. Phys. **96**, 3696 (1992).
[16] Y. Zhu, E. R. Grant, and H. Lefebvre-Brion, J. Chem. Phys. **99**, 2287 (1993).
[17] K. L. Saenger, R. N. Zare, and C. W. Mathews, J. Mol. Spectrosc. **61**, 216 (1976).
[18] P. Labastie, M. C. Bordas, B. Tribollet, and M. Broyer, Phys. Rev. Lett. **52**, 1681 (1984).
[19] S. Fredin, D. Gauyacq, M. Horani, Ch. Jungen, G. Lefèvre, and F. Masnou-Seeuws, Mol. Phys. **60**, 825 (1987).
[20] K. S. Haber, E. Patsilinakou, Y. Jiang, and E. R. Grant, J. Chem. Phys. **94**, 3429 (1991).
[21] T. Huth-Fehre, A. Mank, M. Drescher, N. Böwering, and U. Heinzmann, Phys. Scr. **41**, 454 (1990).